

## Article

# Reactivity of Sulfur and Nitrogen Compounds of FCC Light Cycle Oil in Hydrotreating over CoMoS and NiMoS Catalysts

Jihyun Kim and Yong-Kul Lee \* 

Laboratory of Advanced Catalysis for Energy and Environment, Department of Chemical Engineering, Dankook University, 152 Jukjeon-ro, Yongin 16890, Republic of Korea

\* Correspondence: yolee@dankook.ac.kr

**Abstract:** NiMoS and CoMoS catalysts were synthesized and applied to hydrotreating (HDT) of FCC light cycle oils (FCC-LCO) in an autoclave batch reactor at 613 K and 8.6 MPa H<sub>2</sub>. The S and N compounds in LCO were classified into four and three groups, respectively, in terms of the HDT reactivity. The individual and the competitive reactivities of the S and N compounds in the HDS and the HDN were investigated over the conventional CoMoS and NiMoS catalysts using S and N model compounds (dibenzothiophene, DBT, and carbazole, CBZ). In the HDS of DBT, both the direct desulfurization (DDS) and pre-hydrogenation pathway (HYD) were found to proceed, whereas the HYD pathway was favored for the HDN of CBZ. As a result, the NiMoS catalyst that facilitates the HYD pathway showed better activity in the HDN of LCO than the CoMoS ( $k = 10.20 \times 10^{-2}$  vs.  $1.80 \times 10^{-2} \text{ h}^{-1}$ ). Indeed, the HDS of LCO over the NiMoS was more favorable than that over the CoMoS catalyst ( $k = 4.3 \times 10^{-1}$  vs.  $3.6 \times 10^{-1} \text{ h}^{-1}$ ).

**Keywords:** FCC light cycle oils; NiMoS; CoMoS; hydrotreating; HDS; HDN



**Citation:** Kim, J.; Lee, Y.-K. Reactivity of Sulfur and Nitrogen Compounds of FCC Light Cycle Oil in Hydrotreating over CoMoS and NiMoS Catalysts. *Catalysts* **2023**, *13*, 277. <https://doi.org/10.3390/catal13020277>

Academic Editor: José Antonio Calles

Received: 15 December 2022

Revised: 20 January 2023

Accepted: 24 January 2023

Published: 26 January 2023



**Copyright:** © 2023 by the authors. Licensee MDPI, Basel, Switzerland. This article is an open access article distributed under the terms and conditions of the Creative Commons Attribution (CC BY) license (<https://creativecommons.org/licenses/by/4.0/>).

## 1. Introduction

Light cycle oils (LCO) are produced at the bottom of the fluidized catalytic cracking (FCC) process in a refinery and are enriched with 50–80 wt% heterocyclic aromatic compounds, 3 wt% S, and 600 ppm N [1–4]. It is important to note that LCOs contain polyaromatic hydrocarbons (PAHs), including naphthalene derivatives. Moreover, naphthalene derivatives contain naphthalene, anthracene, and phenanthrene, which can be utilized as the feedstock of benzene, toluene, and xylene (BTX), which are used as raw materials of the petrochemical industry [5–7]. In order to produce high-quality fuels like high-octane gasoline and ultralow sulfur diesel from LCO, the high contents of heterocyclic compounds, such as dibenzothiophene and carbazole derivatives, should be removed to satisfy the environmental restrictions [8–10]. Although both S and N heterocyclic rings are structurally stable, N compounds are more difficult to remove due to the conjugation system in pyridinic or pyrrolic rings [11]. With the growing demands on ultra-low S fuels [4,12,13], research on HDN is becoming more important [14] because N compounds are highly competitive with refractory S compounds over conventional sulfide catalysts, leading to the alleviation of HDS [15].

Although studies of the effect of N compounds on the poisoning of the active centers have been reported [16], the reactivity of different N compounds in terms of types of N rings and alkyl substitution positions has not been verified [17,18]. Therefore, it is vital to demonstrate the HDN reactivity of N compounds in the LCO with respect to the molecular structures and the nature of their competitive reactivity to the HDS. In this study, the S and N compounds in LCO were carefully analyzed, and the individual and competitive reactivities of S and N compounds were investigated over the conventional CoMoS and NiMoS catalysts.

## 2. Results and Discussion

### 2.1. Properties of LCO and Catalyst Samples

Figure 1 displays chromatograms of the aromatic, S, and N compounds in the LCO. Table S1 summarizes the composition of the LCO, which contains 3930 ppm S, 550 ppm N, and 74.3 wt% aromatic compounds with 14.3, 40.6, and 19.4 wt% of mono-, di-, and tri+-aromatics, respectively. Figure 1b shows the GC-SCD chromatography of the LCO, and the corresponding S compounds are listed in Table S2. The S compounds are mostly composed of DBT derivatives and thus can be categorized with respect to the number of alkyl substitutions. For example, Benzothiophen (BT) amounts to 0.7 wt% of the total S in the LCO, followed by BT derivatives with 26.0%, DBT 4.6%, C1-DBT 15.0%, C2-DBT 21.5%, and C3+-DBT 31.4%. Similar results were also reported by U. Nylén et al. [19]. Among the C1-DBT compounds, the amount of 2-/3-MDBT was highest at 7.30 wt%, followed by 6.4% 4-MDBT and 1.3% 1-MDBT. Among the C2-DBT compounds, the amount of 2, 6-/3, 6-DMDBT was highest at 5.5 wt%, followed by 2, 4-DMDBT (2.9%) > 2, 8-/2, 7-/3, 7-DMDBT (2.7) > 4, 6-DMDBT (2.3) > 1, 4-/1, 6-DMDBT (2.2). For the C3-DBT compounds, the amount of 2, 4, 6-TMDBT was highest at 3.4 wt%, followed by 2, 4, 8-/2, 4, 7-TMDBT (1.6%) > 1, 4, 6-TMDBT (1.5) > 3, 4, 6-TMDBT (1.2) > 1, 4, 8-TMDBT (0.8). Figure 1c shows the GC-NPD chromatography of the LCO, and the corresponding N compounds are listed in Table S3. The N compounds are mostly composed of carbazole derivatives and can be classified according to the number of alkyl substituents. For example, carbazole (CBZ) accounts for 4.43 wt% of the total N in LCO, followed by C1-CBZ at 6.28%, C2-CBZ 28.0%, C3+-CBZ 34.4%, and undefined nitrogen compounds 11.4%. Among C1-CBZ, the amount of 1-MCBZ was highest at 6.3 wt%, followed by 3-MCBZ at 4.1%, 2-MCBZ 3.3%, and 4-MCBZ 4.0%. It can be noted that the C1-CBZ fractions were similar to the C1-DBT fractions in Figure 2 [20–22]. Among the C2-CBZ compounds, the amount of 2, 6-/2, 7-DMCBZ was the highest at 5.5 wt%, followed by 1, 4-DMCBZ (4.9) > 1, 5-DMCBZ (4.0) > 2, 4-DMCBZ (3.3) > 1, 8-DMCBZ (2.9) > 2, 5-DMCBZ (2.4) > 1, 2-DMCBZ (1.5) > 3, 5-DMCBZ (1.4). For C3+-CBZ, C3-CBZ was 16.3% of the total C3+-CBZ of 34.4%.

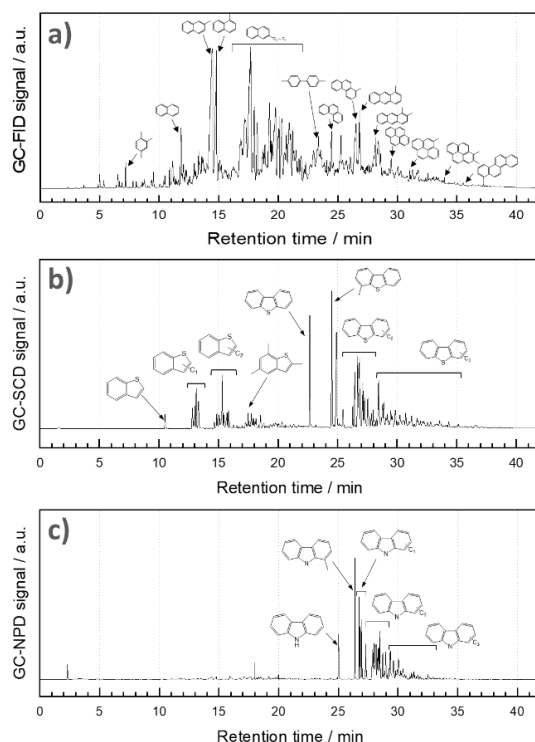


**Figure 1.** GC chromatograms of light cycle oil: (a) aromatic compounds, (b) sulfur compounds, and (c) nitrogen compounds.

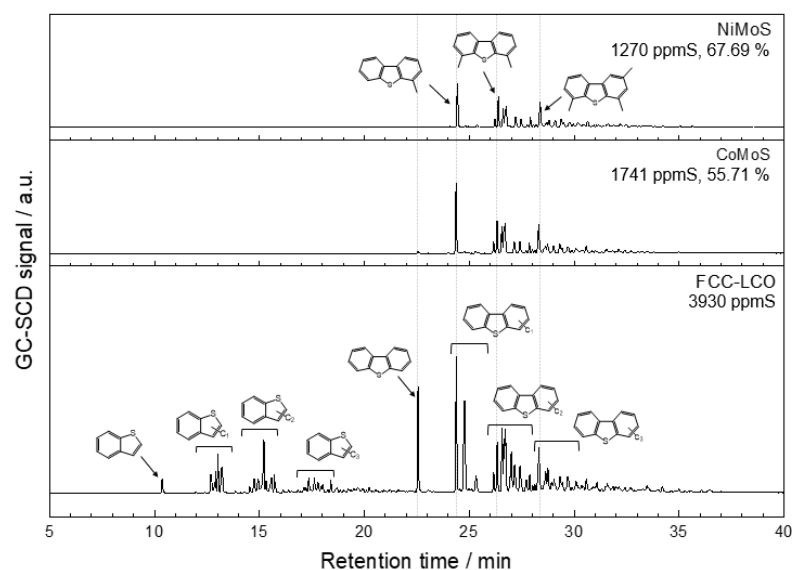


**Figure 2.** S compound distribution in LCO and after 2 h of HDS over CoMoS and NiMoS catalysts at 613 K.

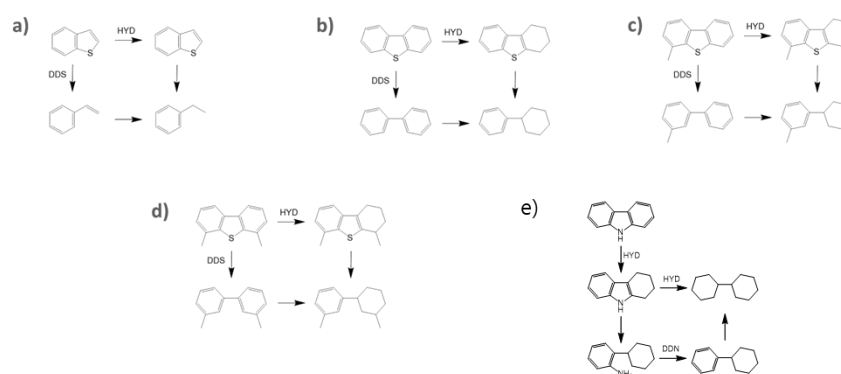
Table S4 summarizes the physical properties of the catalysts used. The BET surface area was measured for the support and catalyst samples, as given in Figure S2. The BET surface area of the  $\gamma$ -Al<sub>2</sub>O<sub>3</sub> is 248.3 m<sup>2</sup>g<sup>-1</sup>. After the CoMo and the NiMo were loaded on the support by impregnation followed by drying and sulfidation, the BET surface area of the CoMoS and the NiMoS were 198.0 m<sup>2</sup>g<sup>-1</sup> and 187.4 m<sup>2</sup>g<sup>-1</sup>, respectively. The mesopore volume of the support became decreased in both cases probably due to the occupation of the CoMo and the NiMo particulates in the mesoporous channel of the support. Moreover, it can be confirmed from the elemental analysis results using ICP that the CoMo and the NiMo were loaded with similar weight percentages.

## 2.2. Reactivity of S Compounds of LCO in HDS over CoMoS and NiMoS Catalyst

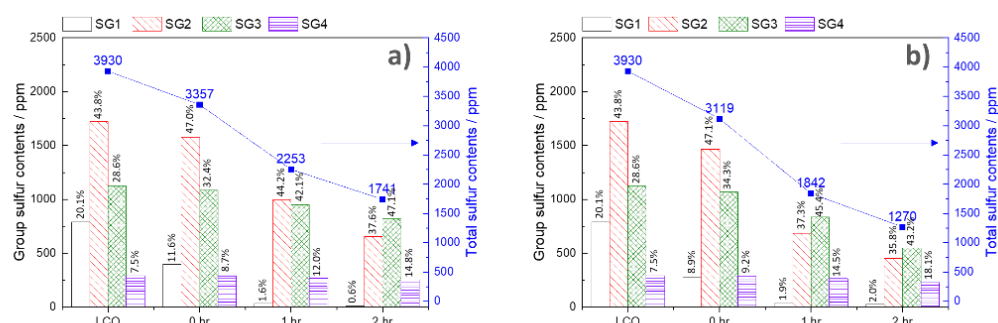
Figure 2 displays the distribution of the S compounds before and after the HDS of LCO over the CoMoS and the NiMoS catalysts. Tables S2 and S5 also list the corresponding S compounds. The total S contents after the HDS over the CoMoS were decreased from 3930 to 1741 ppm S with an overall HDS conversion of 55.7%, but with 67.7% over the NiMoS. For the CoMoS, BT was shown to present the highest HDS conversion of 99.9%, even higher than the overall HDS conversion. As a result, the reaction of BT was too fast to determine the reaction rate constant. DBT underwent a relatively high HDS conversion of 80.8% with a high rate constant of 4.8 h<sup>-1</sup>, even higher than the overall HDS conversion, resulting in a decreased fraction from 4.6 to 2.0% of total S compounds remaining after the HDS. In contrast, 4-MDBT experienced a relatively low HDS conversion of 17.8% with a low rate constant of 0.60 h<sup>-1</sup>, leading to an increased fraction from 6.4 to 11.9% of total S compounds remaining after the HDS. More importantly, 4,6-DMDBT, known as the most refractory S compound in petroleum feedstocks, experienced the lowest HDS conversion of 4.2%, even lower than that of 4-MDBT, being more than doubled in the fraction from 2.3 to 4.9% of total S compounds remaining after the HDS. These results suggest that it would be desirable to categorize the S compounds in LCO depending on the reactivity in the HDS rather than on the molecular weight or structure.

Mochida et al. [23] classified S compounds in gas oils into four groups based on the HDS reactivity in which the representative S compounds were BT, DBT, 4-MDBT, and 4, 6-DMDBT, corresponding to the sulfur group 1 (SG1), 2 (SG2), 3 (SG3), and 4 (SG4), respectively (Figure 3). In a similar manner, the S compounds in the feed and products after the HDS were classified into four groups in terms of the HDS reactivity, as given in Figure 4 and Table S5. The S compounds of LCO were composed of 20.1% SG1, 43.8% SG2,

28.6% SG3, and 7.5% SG4, as shown in Figure 4a. In the case of SG1, the fraction of SG1 remaining after the HDS over the CoMoS decreased from 20.1% in the feed to 0.6% in the product after 2 h of reaction. Over the NiMoS<sub>2</sub>, the fractions showed similar behaviors as those of the CoMoS. These results indicate that most of the S compounds of SG1 are removed after the HDS. The fraction of the S compounds in SG2 slightly increased from 43.8% to 47.0%, and then decreased again to 44.4 and 37.6%. Due to the slower HDS rates for SG2, 3, and 4 than SG1, the S fractions belonging to SG2~4 were found to be higher at the beginning of the HDS. In SG3 and SG4, the fraction of the S compounds after the HDS over the CoMoS increased. These results indicate that the S compounds of SG3 decrease slowly, and those of SG4 are hardly removed. The CoMoS thus turned out to be effective in removing less sterically hindered S compounds (SG1 and 2), while it showed a low activity toward refractory S compounds belonging to SG3 and SG4. These results are in line with the previous studies in the literature. For example, the HDS of BT could be suggested by two reaction pathways resulting in the presence of styrene or ethyl benzene in the product [24]. The HDS of thiophenic compounds, having a weak C-S bond, could directly result in S removal without the saturation of the heteroatom ring. The HDS of DBT could follow two parallel desulfurization pathways, which removes S as H<sub>2</sub>S, leading to the major products of biphenyl for the DDS and hexahydro-dibenzothiophene for the HYD. The HDS of the refractory compounds, such as 4-MDBT and 4,6-DMDBT, is often required for deep HDS (Figure 3). Generally, the reactivity of these compounds is low due to steric hindrance of the transition state inhibiting the C-S bond cleavage through the DDS pathway. The reactivity of 4-MDBT and 4,6-DMDBT could be improved by increasing the HYD activity of the catalysts [25,26]. It can be noted that the reactivity of SG3 and SG4 over the NiMoS<sub>2</sub> was twice more than those over the CoMoS, as given in Table S5.



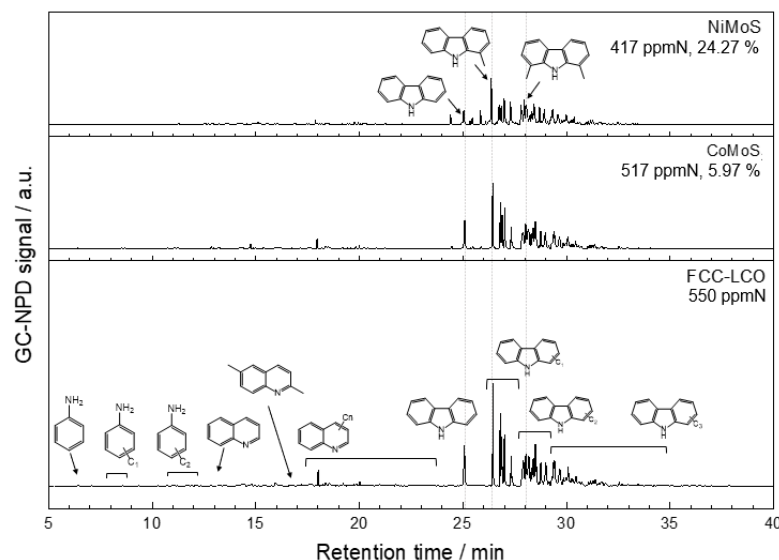
**Figure 3.** Reaction pathway for HDS of (a) benzothiophene (BT), (b) dibenzothiophene (DBT), (c) 4-methyl dibenzothiophene (4-MDBT), and (d) 4,6-dimethyl dibenzothiophene (4,6-DMDBT), and (e) HDN of carbazole (CBZ).



**Figure 4.** The fraction of the S compounds of SG1, 2, 3, and 4 in the LCO and the products after the HDS over (a) CoMoS and (b) NiMoS.

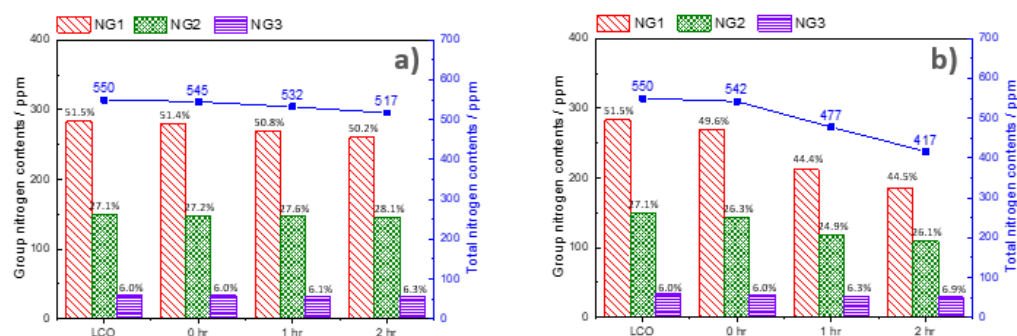
### 2.3. Reactivity of N Compounds of LCO in HDS over CoMoS and NiMoS Catalyst

Figure 5 displays the distributions of the N compounds before and after the HDN of LCO over the CoMoS and NiMoS catalysts. After the HDN, the total N contents were decreased from 550 to 517 ppm N with the overall HDN conversions of 6.0% over the CoMoS, and to 417 ppm N with the HDN conversion of 24.3% over the NiMoS. In Table S6, the kinetic constants of the overall HDN of the NiMoS<sub>2</sub> were five times higher than those of the CoMoS. These results are consistent with previous studies [11,12,27–29]. The N compounds can be divided into two groups according to the degree of basicity: basic N and non-basic N. Basic N compounds contain the six-membered pyridinic ring, and the other N compounds contain the five-membered pyrrolic ring. The HDS generally does not require the complete HYD of the ring prior to the hydrogenation, while the HYD in the HDN of heterocyclic N compounds is often inevitable due to the conjugation system of the N-rings [30]. The reaction scheme for the HDN of carbazole (CBZ) is shown in Figure 3 [31,32]. CBZ undergoes the HYD pathway, producing tetrahydro-carbazole (THC). The HDN of THC then follows two parallel denitrogenation pathways, leading to the major products of bicyclohexyl (BCH) and cyclohexyl aniline (CHA) via the direct denitrogenation (DDN) and HYD, respectively.



**Figure 5.** N compound distribution in LCO and after 2 h of HDN over CoMoS and NiMoS catalysts at 613 K.

Figure 6 displays the N fractions before and after the HDN. Table S6 also summarizes the N fractions of the N compounds. It can be seen that the CBZ shows a relatively high HDN conversion of 46.2%, even higher than the overall HDN conversion of 24.3% over the NiMoS, resulting in a decreased fraction from 4.4 to 3.3% of the total N compounds remaining after the HDN. The HDN conversion of 1-MCBZ was a little low at 27.4%, resulting in a consistent fraction from 6.3 to 6.2%. In contrast, 1,8-DMCBZ experienced the lowest HDN conversion of 0.5%, raising the N fraction from 2.9 to 3.9% of total N compounds remaining after the HDN. These results thus suggested that it would be desirable to categorize the N compounds based on the reactivity in the HDN, as the case in the HDS of S compounds in the LCO.



**Figure 6.** The fraction of the N compounds of NG1, 2, and 3 in the LCO and the products after the HDN over (a) CoMoS and (b) NiMoS.

In a similar manner, the N compounds in the feed and products after the HDN were classified into three groups in terms of HDN reactivity over the NiMoS catalyst at 8.6 MPa and 613 K. The N compounds were classified with respect to the level of the kinetic rate constants of the N compounds, where the rate constant of NG1 was over  $1.20 \times 10^{-1} \text{ h}^{-1}$ , followed by NG2 with  $0.60 \times 10^{-1} \sim 1.20 \times 10^{-1}$ , and NG3 with  $<0.60 \times 10^{-1}$ . The N compounds that belong to NG1 were CBZ and alkyl-substituted CBZs such as 2-/3-/4-MCBZ, and 2,6-/2,7-/3,5-/2,4-/2,5-DMCB, which showed a similar reactivity in the HDN with CBZ, leading to a relatively high HDN conversion. The N compounds belonging to NG2 were 1-MCBZ and its alkyl-substituted 1-MCBZs such as 1,4-/1,5-/1,2-DMCBZ. The N compounds belonging to NG3 were 1, 8-DMCBZ, and its alkyl-substituted derivatives. As displayed in Figure 6, the N compounds of NG2 showed a high HDN conversion, resulting in a lower N fraction after the HDN. In NG2, the fraction of the N compounds after the HDN over the NiMoS was comparable to those in the feed. In contrast, the N compounds of NG3 were found to remain almost unconverted after the HDN.

#### 2.4. HDS and HDN Reaction Mechanism of Model Feed over NiMoS Catalyst

Figure 7 shows the HDS and HDN profiles of each N group, and Table S7 lists the rate constants in the HDS and HDN over the NiMoS<sub>2</sub> catalyst. The conversion of DBT and CBZ could be described by the parallel reaction networks, which followed a pseudo first-order reaction. The equations are listed below, which include the relative concentrations of the reactant and product species as the function of reaction time:

(1) HDN of CBZ

$$\frac{dC_{\text{CBZ}}}{dt} = -k_{11}C_{\text{CBZ}} \quad (1)$$

$$\frac{dC_{\text{THC}}}{dt} = k_{11}C_{\text{CBZ}} - k_{12}C_{\text{THC}} - k_{13}C_{\text{THC}} \quad (2)$$

$$\frac{dC_{\text{CHA}}}{dt} = k_{13}C_{\text{THC}} - k_{14}C_{\text{CHA}} \quad (3)$$

$$\frac{dC_{\text{CHB}}}{dt} = k_{14}C_{\text{CHA}} - k_{15}C_{\text{CHB}} \quad (4)$$

$$\frac{dC_{\text{BCH}}}{dt} = k_{12}C_{\text{THC}} + k_{15}C_{\text{CHB}} \quad (5)$$

(2) HDS of DBT

$$\frac{dC_{\text{DBT}}}{dt} = -k_{21}C_{\text{DBT}} \quad (6)$$

$$\frac{dC_{\text{BP}}}{dt} = k_{21}C_{\text{DBT}} - k_{21}C_{\text{BP}} \quad (7)$$

$$\frac{dC_{CHB}}{dt} = k_{22}C_{BP} - k_{23}C_{CHB} \quad (8)$$

$$\frac{dC_{BCH}}{dt} = k_{23}C_{CHB} \quad (9)$$

### (3) Combined HDT of CBZ and DBT

$$\frac{dC_{DBT}}{dt} = -k_{31}C_{DBT} \quad (10)$$

$$\frac{dC_{BP}}{dt} = k_{31}C_{DBT} - k_{32}C_{BP} \quad (11)$$

$$\frac{dC_{CHB}}{dt} = k_{32}C_{BP} + k_{37}C_{CHA} - k_{33}C_{CHB} \quad (12)$$

$$\frac{dC_{CBZ}}{dt} = -k_{34}C_{CBZ} \quad (13)$$

$$\frac{dC_{THC}}{dt} = k_{34}C_{CBZ} - k_{36}C_{THC} - k_{35}C_{THC} \quad (14)$$

$$\frac{dC_{CHA}}{dt} = k_{36}C_{THC} - k_{37}C_{CHA} \quad (15)$$

$$\frac{dC_{BCH}}{dt} = k_{33}C_{CHB} + k_{35}C_{THC} \quad (16)$$

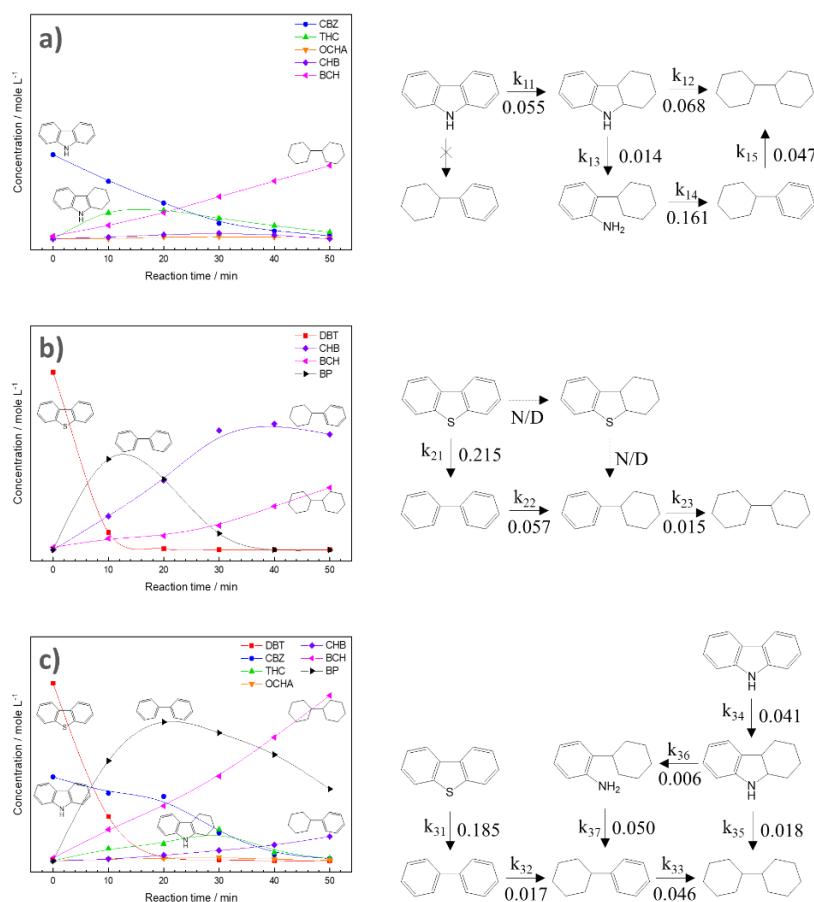


**Figure 7.** Concentrations of products as a function of time during HDS of DBT and HDN of CBZ over NiMoS: (a) HDN of 100 ppm N CBZ, (b) HDS of 500 ppm S DBT, and (c) Combined HDN and HDS of 100 ppm N CBZ and 500 ppm S DBT.

The subscripts denote the species observed in the reactions: CBZ: carbazole, THC: tetrahydro carbazole, OCHA: ortho-cyclohexyl aniline, CHB: cyclohexyl benzene, BCH: bicyclohexyl, DBT: dibenzothiophene, BP: biphenyl.

Figure 7a shows that the C-N cleavage reaction rate from THC to OCHA was the rate-determining step, indicating the HYD pathway was favored for the HDN of the CBZ. In addition, it could be confirmed that the reaction rate of DBT is faster than that of CBZ [33]. In Figure 7b, the formation of BP (biphenyl) was dominant at the early stage of the reaction, indicating that the DDS pathway of DBT is dominant. The result is in accordance with a previous study, in which the NiMoS catalyst prefers the DDS pathway in the absence of alkyl groups on the S compounds [34]. Figure 7c compares the reaction rates of the CBZ and DBT mixture. It can be observed that the reaction rate of DBT was found to decrease by 14%, and the reaction rate of CBZ was decreased by 25%, indicating that the N compounds following the HYD pathway were more affected in the competitive hydrotreating than DBT favoring the DDS pathway (Table S7). These results suggested that the DDS and the HYD could proceed on the same active site. Considering that the reaction rate of CBZ decreased more than that of DBT, there might be more hydrogenation sites available on the NiMoS, and the adsorption of DBT could be stronger than that of CBZ.

### 3. Experimental

#### 3.1. Materials

The FCC-LCO as a feedstock was supplied from a refinery in South Korea, and the specification is summarized in Table S1. Nickel (II) nitrate hexahydrate (Alfa Aesar, 98%), cobalt nitrate hexahydrate (Kanto chemical, 99.5%), and ammonium molybdate tetrahydrate (Samchun chemical, 99.0%) were used as precursors to prepare the catalyst samples.  $\gamma$ -Al<sub>2</sub>O<sub>3</sub> pellets (Alfa Aesar, 255 m<sup>2</sup>·g<sup>-1</sup>) were sieved to make a uniform powder (45~75  $\mu$ m) as catalyst supports. The  $\gamma$ -Al<sub>2</sub>O<sub>3</sub>-supported CoMoS and NiMoS catalysts were prepared by incipient wetness impregnation of the alumina support with an aqueous solution, in which the amount of metal loading was fixed at 3 wt% active metal and 8 wt% Mo. After completing the impregnation, the mixture was dried overnight at 373 K, and then calcined at 673 K for 4 h. Prior to the reaction, the catalysts were sulfided for 2 h via decomposition of dimethyl disulfide in tridecane (S: 5%) at 653 K, and were cited as CoMoS and NiMoS catalysts. The catalysts were stored in n-hexane to avoid air exposure.

#### 3.2. Characterization of Catalyst

N<sub>2</sub> physisorption of the samples was measured on a Micromeritics ASAP 2060 micropore size analyzer. The surface area of the sample was obtained by the linear portion of BET plots ( $P/P_0 = 0.05$ – $0.35$ ) at 77 K. Approximately 0.1 g of catalyst was placed in a quartz tube. Before the measurement, the sample was degassed at 403 K overnight and then cooled to room temperature. The chemical composition of the samples was determined by inductively coupled plasma-atomic emission spectroscopy (ICP-AES) (PerkinElmer, Model Optima 8300).

#### 3.3. Activity Tests

For the reaction test, the feed mixture of 30 g LCO and 0.3 g catalyst samples was loaded into a 150 mL autoclave (Hanwool Engineering, Uiwang, Korea). The mixture was heated to 353 K with bubbling H<sub>2</sub> at 1000 rpm. The reactor was then filled with H<sub>2</sub> to 6.0 MPa at 353 K, which was heated to 613 K at 10 K·min<sup>-1</sup> and the H<sub>2</sub> pressure was increased to 8.6 MPa.

Liquid products were quantified by a gas chromatograph equipped with a sulfur chemiluminescence detector (Agilent-355 SCD, HP-1) to monitor the distribution of sulfur compounds, on samples collected at 0.5 h intervals. The product composition at reaction time 0 h was determined from the product after cooling the reactor as soon as the reaction temperature was reached. 4, 6-dimethyldibenzothiophene (4, 6-DMDBT), 4-methyl benzothiophene (4M-DBT), benzothiophene (BT), and dibenzothiophene (DBT) were used

as model sulfur compounds. The N compounds distribution in the feed and products were quantified using a gas chromatograph (GC6890, Agilent) equipped with a nitrogen phosphorus detector (NPD). Pyridine, indole, quinoline, and carbazole were used as model nitrogen compounds. The reaction conversions for HDS and HDN were defined as the percent of total S and N removal from those in the feed LCO. Model feeds were also applied to carried out kinetic studies using 100 ppm N CBZ and 500 ppm S DBT in tridecane at the same reaction conditions with collecting liquid product samples at 10 min intervals. The reaction rates and kinetic parameters for each proposed reaction pathway were estimated using the parameter estimation algorithm, and all calculation was performed with MATLAB version 2019a. The reaction equations were treated with the integration methods, and non-linear regression was conducted using the “trust-region-reflective” method.

#### 4. Conclusions

The hydrotreating of LCO was conducted in an autoclave batch reactor at 613 K and 8.6 MPa H<sub>2</sub>. The S compounds of LCO were classified into four groups in terms of the reactivity in the HDS reaction: the highest reactive S group of alkyl-BTs (SG1), the sterically less hindered alkyl-DBTs (SG3), and the lowest reactive S group of sterically hindered DBT derivatives (SG4). Similarly, the N compounds of LCO were classified into three groups in terms of the reactivity in the HDN, from the highest reactive N group of alkyl-CBZs (NG1) to the lowest reactive N group of alkyl-CBZs (NG3). It was noted that the steric hindrance of N compounds belonging to NG3, like 1, 8-dimethylcarbazole (1, 8-DMCBZ), could lead to poor reactivity in the HDN, as also observed in the HDS. It was suggested that the NiMoS catalyst could be superior over the CoMoS catalysts in the HDS and the HDN of LCO by facilitating the hydrogenation pathway to mitigate the steric hindrance of the refractory S and N compounds.

**Supplementary Materials:** The following supporting information can be downloaded at: <https://www.mdpi.com/article/10.3390/catal13020277/s1>, Figure S1. The structure of heterocyclic aromatic compounds with labeled C atoms: (a) benzothiophene, (b) dibenzothiophene, and (c) carbazole; Figure S2. N<sub>2</sub> adsorption isotherm plot of (a) CoMoS and (b) NiMoS; Table S1. Composition and properties of light cycle oil (LCO); Table S2. Sulfur distribution of LCO; Table S3. Nitrogen distribution of LCO; Table S4. Physical properties of the support and catalysts; Table S5. Group of S compounds in LCO and hydrotreated LCO at 613 K; Table S6. Group of N compounds in LCO and hydrotreated LCO at 613 K; Table S7. Rate constants during HDN of CBZ and HDS of DBT over the NiMoS.

**Author Contributions:** Y.-K.L. conceived and designed the experiments; J.K. performed the experiments; J.K. and Y.-K.L. wrote the paper. All authors have read and agreed to the published version of the manuscript.

**Funding:** This research received no external funding.

**Data Availability Statement:** Experimental data will be available upon request.

**Conflicts of Interest:** The authors declare no conflict of interest. The funding sponsors had no role in the design of the study; in the collection, analyses, or interpretation of data; in the writing of the manuscript, and in the decision to publish the results.

#### References

1. Song, C.; Hsu, C.; Mochida, I. *Chemistry of Diesel Fuels*; CRC Press: Boca Raton, FL, USA, 2020.
2. Corma, A.; Alfarob, V.; Orchillés, A. Decalin and tetralin as probe molecules for cracking and hydrotreating the light cycle oil. *J. Catal.* **2001**, *200*, 34–44. [[CrossRef](#)]
3. Yun, G.-N.; Cho, K.-S.; Kim, Y.-S.; Lee, Y.-K. A New Approach to Deep Desulfurization of Light Cycle Oil over Ni<sub>2</sub>P Catalysts: Combined Selective Oxidation and Hydrotreating. *Catalysts* **2018**, *8*, 102. [[CrossRef](#)]
4. Cho, K.-S.; Lee, Y.-K. Effects of nitrogen compounds, aromatics, and aprotic solvents on the oxidative desulfurization (ODS) of light cycle oil over Ti-SBA-15 catalyst. *Appl. Catal. B Environ.* **2014**, *147*, 35–42. [[CrossRef](#)]
5. Laredo, G.; Pérez-Romo, P.; Escobar, J.; Garcia-Gutierrez, J.; Vega-Merino, P. Light Cycle Oil Upgrading to Benzene, Toluene, and Xylenes by Hydrocracking: Studies Using Model Mixtures. *Ind. Eng. Chem. Res.* **2017**, *56*, 10939–10948. [[CrossRef](#)]

6. Laredo, G.; Merino, P.V.; Hernández, P. Light Cycle Oil Upgrading to High Quality Fuels and Petrochemicals: A Review. *Ind. Eng. Chem. Res.* **2018**, *57*, 7315–7321. [[CrossRef](#)]
7. Kim, Y.-S.; Cho, K.-S.; Lee, Y.-K. Morphology effect of  $\beta$ -zeolite supports for Ni2P catalysts on the hydrocracking of polycyclic aromatic hydrocarbons to benzene, toluene, and xylene. *J. Catal.* **2017**, *351*, 67–78. [[CrossRef](#)]
8. Oh, Y.; Shin, J.; Noh, H.; Kim, C.; Kim, Y.-S.; Lee, Y.-K.; Lee, J.K. Selective hydrotreating and hydrocracking of FCC light cycle oil into high-value light aromatic hydrocarbons. *Appl. Catal. A Gen.* **2019**, *577*, 86–98. [[CrossRef](#)]
9. Tao, L.; Fairley, D.; Kleeman, M.J.; Harley, R.A. Effects of Switching to Lower Sulfur Marine Fuel Oil on Air Quality in the San Francisco Bay Area. *Environ. Sci. Technol.* **2013**, *47*, 10171–10178. [[CrossRef](#)]
10. Deniz, C.; Zincir, B. Environmental and economical assessment of alternative marine fuels. *J. Clean. Prod.* **2016**, *113*, 438–449. [[CrossRef](#)]
11. Song, C.; Ma, X. New design approaches to ultra-clean diesel fuels by deep desulfurization and deep dearomatization. *Appl. Catal. B Environ.* **2003**, *41*, 207–238. [[CrossRef](#)]
12. Azizi, N.; Ali, S.; Alhooshani, K.; Kim, T.; Lee, Y.; Park, J.I.; Miyawaki, J.; Yoon, S.; Mochida, I. Hydrotreating of light cycle oil over NiMo and CoMo catalysts with different supports. *Fuel Process. Technol.* **2013**, *109*, 172–178. [[CrossRef](#)]
13. Yun, G.-N.; Lee, Y.-K. Dispersion effects of Ni2P catalysts on hydrotreating of light cycle oil. *Appl. Catal. B Environ.* **2014**, *150–151*, 647–655. [[CrossRef](#)]
14. Oyama, S.T.; Lee, Y.-K. Mechanism of Hydrodenitrogenation on Phosphides and Sulfides. *J. Phys. Chem. B* **2005**, *109*, 2109–2119. [[CrossRef](#)] [[PubMed](#)]
15. Furimsky, E.; Massoth, F. Hydrodenitrogenation of Petroleum. *Catal. Rev.* **2005**, *47*, 297–489. [[CrossRef](#)]
16. Laredo, G.; Altamirano, E.; De los Reyes, J. Self-inhibition observed during indole and o-ethylaniline hydrogenation in the presence of dibenzothiophene. *Appl. Catal. A Gen.* **2003**, *242*, 311–320. [[CrossRef](#)]
17. Fu, C.; Schaffer, A. Effect of nitrogen compounds on cracking catalysts. *Ind. Eng. Chem. Prod. Res. Dev.* **1985**, *24*, 68–75. [[CrossRef](#)]
18. Kwak, C.; Lee, J.; Bae, J.; Moon, S. Poisoning effect of nitrogen compounds on the performance of CoMoS/Al<sub>2</sub>O<sub>3</sub> catalyst in the hydrodesulfurization of dibenzothiophene, 4-methyldibenzothiophene, and 4,6-dimethyldibenzothiophene. *Appl. Catal. B Environ.* **2001**, *35*, 59–68. [[CrossRef](#)]
19. Nylén, U.; Delgado, J.; Järås, S.; Boutonnet, M. Characterization of alkylated aromatic sulphur compounds in light cycle oil from hydrotreated vacuum gas oil using GC-SCD. *Fuel Process. Technol.* **2004**, *86*, 223–234. [[CrossRef](#)]
20. Li, M.; Larter, S.; Stoddart, D.; Bjoroy, M. Liquid chromatographic separation schemes for pyrrole and pyridine nitrogen aromatic heterocycle fractions from crude oils suitable for rapid characterization of geochemical samples. *Anal. Chem.* **1992**, *64*, 1337–1344. [[CrossRef](#)]
21. Li, X.; Gao, Y.; Zuo, C.; Zheng, S.; Xu, F.; Sun, Y.; Zhang, Q. The Gas-Phase Formation Mechanism of Dibenzofuran (DBF), Dibenzothiophene (DBT), and Carbazole (CA) from Benzofuran (BF), Benzothiophene (BT), and Indole (IN) with Cyclopentadienyl Radical. *Int. J. Mol. Sci.* **2019**, *20*, 5420. [[CrossRef](#)]
22. Dorbon, M.; Ignatiadis, I.; Schmitter, J.-M.; Arpino, P.; Guiochon, G.; Toulhoat, H.; Huc, A. Identification of carbazoles and benzocarbazoles in a coker gas oil and influence of catalytic hydrotreatment on their distribution. *Fuel* **1984**, *63*, 565–570. [[CrossRef](#)]
23. Ma, X.; Sakanishi, K.; Mochida, I. Hydrodesulfurization Reactivities of Various Sulfur Compounds in Diesel Fuel. *Ind. Eng. Chem. Res.* **1994**, *33*, 218–222. [[CrossRef](#)]
24. Kilanowski, D.; Teeuwen, H.; de Beer, V.; Gates, B.; Schuit, G.; Kwart, H. Hydrodesulfurization of thiophene, benzothiophene, dibenzothiophene, and related compounds catalyzed by sulfided CoOMoO<sub>3</sub>-Al<sub>2</sub>O<sub>3</sub>: Low-pressure reactivity studies. *J. Catal.* **1978**, *55*, 129–137. [[CrossRef](#)]
25. Pérot, G. Hydrotreating catalysts containing zeolites and related materials—Mechanistic aspects related to deep desulfurization. *Catal. Today* **2003**, *86*, 111–128. [[CrossRef](#)]
26. Breyse, M.; Djega-Mariadassou, G.; Pessayre, S.; Geantet, C.; Vrinat, M.; Pérot, G.; Lemaire, M. Deep desulfurization: Reactions, catalysts and technological challenges. *Catal. Today* **2003**, *84*, 129–138. [[CrossRef](#)]
27. Song, C. An overview of new approaches to deep desulfurization for ultra-clean gasoline, diesel fuel and jet fuel. *Catal. Today* **2003**, *86*, 211–263. [[CrossRef](#)]
28. Laredo, G.; Montesinos, A.; De Los Reyes, J. Inhibition effects observed between dibenzothiophene and carbazole during the hydrotreating process. *Appl. Catal. A Gen.* **2004**, *265*, 171–183. [[CrossRef](#)]
29. García-Martínez, J.; Castillo-Araiza, C.; De los Reyes Heredia, J.; Trejo, E.; Montesinos, A. Kinetics of HDS and of the inhibitory effect of quinoline on HDS of 4,6-DMDBT over a Ni-Mo-P/Al<sub>2</sub>O<sub>3</sub> catalyst: Part I. *Chem. Eng. J.* **2012**, *210*, 53–62. [[CrossRef](#)]
30. Finiels, A.; Geneste, P.; Moulinas, C.; Olive, J. Hydroprocessing of secondary amines over NiW-Al<sub>2</sub>O<sub>3</sub> Catalyst. *Appl. Catal.* **1986**, *22*, 257–262. [[CrossRef](#)]
31. Szymańska, A.; Lewandowski, M.; Sayag, C.; Djéga-Mariadassou, G. Kinetic study of the hydrodenitrogenation of carbazole over bulk molybdenum carbide. *J. Catal.* **2003**, *218*, 24–31. [[CrossRef](#)]
32. Nagai, M.; Goto, Y.; Irisawa, A.; Omi, S. Catalytic Activity and Surface Properties of Nitrided Molybdena-Alumina for Carbazole Hydrodenitrogenation. *J. Catal.* **2000**, *191*, 128–137. [[CrossRef](#)]

33. Zepeda, T.; Pawelec, B.; Obeso-Estrella, R.; de León, J.D.; Fuentes, S.; Alonso-Núñez, G.; Fierro, J. Competitive HDS and HDN reactions over NiMoS/HMS-Al catalysts: Diminishing of the inhibition of HDS reaction by support modification with P. *Appl. Catal. B Environ.* **2016**, *180*, 569–579. [[CrossRef](#)]
34. Kagami, N.; Vogelaar, B.; van Langeveld, A.; Moulijn, J. Reaction pathways on NiMo/Al<sub>2</sub>O<sub>3</sub> catalysts for hydrodesulfurization of diesel fuel. *Appl. Catal. A Gen.* **2005**, *293*, 11–23. [[CrossRef](#)]

**Disclaimer/Publisher's Note:** The statements, opinions and data contained in all publications are solely those of the individual author(s) and contributor(s) and not of MDPI and/or the editor(s). MDPI and/or the editor(s) disclaim responsibility for any injury to people or property resulting from any ideas, methods, instructions or products referred to in the content.